RSC Advances

PAPER

View Article Online
View Journal | View Issue

Cite this: *RSC Adv.*, 2022, **12**, 29602

Aptasensing of ciprofloxacin residue using graphene oxide modified with gold nanoparticles and branched polyethyleneimine†

Mansour Mahmoudpour,[ab] Jafar Ezzati Nazhad Dolatabadi,[c] Mohammad Hasanzadeh,*[ad] Aziz Homayouni Rad,[b] Mohammadali Torbati*[b] and Farzad Seidi[e]

Precise monitoring of antibiotic residues in aqueous solution is of vital significance for safeguarding the environment and food resources. Herein, a convenient platform was fabricated for the electrochemical assay of ciprofloxacin (CFX) in real milk samples using aminated aptamer and graphene oxide nanogold-functionalized branched polyethyleneimine (GO-PEI-AuNPs) nanocomposite. For the first time, a gold electrode was modified with GO-PEI-AuNPs. The modified surface endowed excellent electrochemical substrates with large surface areas, excellent electron transfer rates, and suitable capabilities to firmly attach high amounts of aptamer. After further modification of substrate with CFX specific aptamer a recognition probe enabling selective and sensitive determination of CFX was realized. All of the aptasensor fabrication steps were surveyed *via* cyclic voltammetry techniques. The construction and morphology of the GO-PEI-AuNPs composite were evaluated by UV-Vis spectroscopy, transmission electron microscopy, and field emission scanning electron microscopy. Under optimal conditions, the suggested scaffold can offer an acceptable linear range of 0.001 to 100 μM and a low limit of quantification of 0.001 μM for selective and sensitive monitoring of CFX in real samples. The effectiveness of the apta-assay was confirmed by detection of CFX in pasteurized and local milk samples for which suitable analytical results were achieved. It is expected that the developed substrate can be facilely extended to other aptamer-based multiplex screening platforms in actual food and environmental samples.

Received 1st May 2022
Accepted 3rd October 2022

DOI: 10.1039/d2ra02761e

rsc.li/rsc-advances

1. Introduction

Ciprofloxacin (CFX) as one of the most significant second-generation quinolone antibiotics, is broadly used in anti-infective treatment in livestock, poultry and aquaculture owing to quick and broad-spectrum bactericidal or bacteriostatic activity, low cross-resistance and low price.[1] Nevertheless, its abuse has led to CFX residues in animal-derived foodstuffs because of its slow degradation and poor metabolism. CFX residues cause a series of concerns such as antibiotic resistance, disorders of intestinal flora, toxicity and allergic reactions that are hazards to public health.[2,3] Hence, the maximum level of CFX in various foodstuffs has been limited by the European Union (EU) like the MRL of CFX in fish must be lower than 100 μg kg^{-1}.[4] From this perspective, cutting-edge antibiotic sensing technologies are of great importance to avoid the risk of CFX residues in the diverse complex food matrix and guarantee human safety.[5,6] Current standard methods for exploring antibiotic residues could be separated into laboratory instrumental systems and portable sensing techniques. Though chromatography-based methods as the chief instances of instrumental essays can quantitatively identify CFX in good accuracy and high sensitivity, they rely on long operation times, intricate operations and expensive equipment.[7] Besides, various quantities of toxic solvent wastes are typically produced, making these approaches a less eco-friendly option. Therefore, there is a grim need to consider substitute methodologies for monitoring antibiotic residues in a highly-sensitive, rapid, easy-to-operate, specific, and user-friendly way.[8,9]

Aptamers is short single-stranded RNA, DNA or modified nucleic acids which could fold into particular secondary or tertiary constructions upon coupling to their target molecules. Owing to the benefits of cost-effectiveness, ease of synthesis/chemical modification, and smaller size, aptamers have earned

[a]*Pharmaceutical Analysis Research Center, Tabriz University of Medical Sciences, Tabriz, Iran. E-mail: hasanzadehm@tbzmed.ac.ir*

[b]*Department of Food Science and Technology, Faculty of Nutrition and Food Sciences, Nutrition Research Center, Tabriz University of Medical Sciences, Tabriz, Iran. E-mail: torbatima@yahoo.com*

[c]*Drug Applied Research Center, Tabriz University of Medical Sciences, Tabriz, Iran*

[d]*Nutrition Research Center, Tabriz University of Medical Sciences, Tabriz, Iran*

[e]*Jiangsu Co-Innovation Center for Efficient Processing and Utilization of Forest Resources and International Innovation Center for Forest Chemicals and Materials, Nanjing Forestry University, Nanjing 210037, China*

† Electronic supplementary information (ESI) available. See DOI: https://doi.org/10.1039/d2ra02761e

popularity over antibodies in terms of designing ideal configurations to selectively detect targeting objects.[10,11] Among different sensing methods, electrochemical aptasensors, as an efficient bioanalysis technique, remove the traditional analytical matters since they offer highly selective and sensitive detection with quick response time, while presenting significant prospective in environmental monitoring and food quality control.[12]

A current progress in the design of an aptasensors have confirmed that incorporating aptamers with advanced nanomaterials lead to the sensing nanoprobes with paramount sensitivity, which in turn is ideal in monitoring of antibiotics residues. Actually, these materials with nano-scale dimensions provide a superlative substrate for a sufficient immobilization of aptamers, which is an important step in the designing of nanoprobes.[13] Therefore, the one-step analysis with label-free assays, reagent-free (in some cases), high sensitivity, and requiring a small sample volume could be realized.[14] In this point, different types of nanostructures were advanced and applied on the working electrode for enhancing aptamers coating amount. The 2D planar construction of graphene together with its large surface area and superb electrical conductivity make it an excellent nanomaterial in electrochemical sensing.[15] This nanoparticle is highly stable, and the chemical reaction is inert. The agglomeration happens facilely owing to the strong van der Waals forces between layers. These qualities are not favorable to the investigation and operation of graphene. Since graphene oxide (GO) comprises abundant oxygen-containing groups such as epoxy, carboxyl and hydroxyl groups, the GO could be covalently activated *via* other molecules. The activated GO exhibited excellent dispersibility that can expand the accessibility of graphene.[16] Polyethylene imine (PEI), as a synthetic polycations, is an aliphatic, weak base and non-toxic composite that was

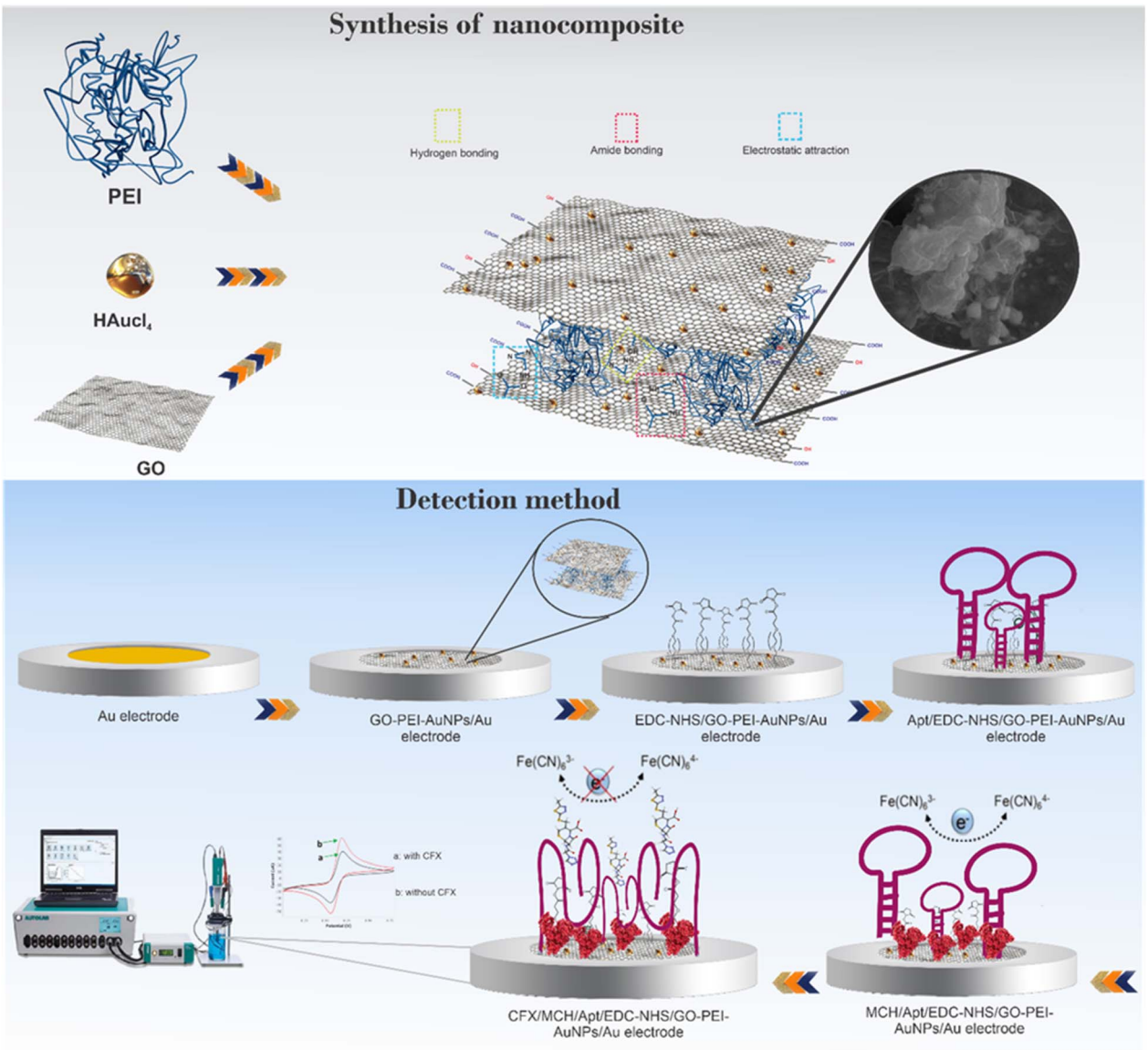

Scheme 1 Schematic illustration of the fabrication process of the GO-PEI-AuNPs/AuE modified electrode and the electrochemical aptasensor for measuring the CFX concentration.

synthesized by bonding of ethylene imine elements. Indeed, PEI, a water-soluble polymer whose branches and backbone both have plentiful reactive amine groups that can be easily chemically react *via* hydrogen bonding with the other materials comprising epoxy or carboxyl groups.[17] Accordingly, water-dispersible polyethyleneimine functionalized graphene (PEI-G) nanocomposite was designed herein by a facile, cost-effective, and eco-friendly process. Likewise, metal nanomaterials can be incorporated on the GO-PEI surface. Recently, polymer-assisted production of metal nanomaterials has ignited a surge of unprecedented attention because of it causes efficiently nanoparticles stabilization *via* acting as both a reducing and stabilizer agent to successfully provide monodispersed units.[18] Today, linear PEI was used as both a protecting and reducing/stabilizing agent in designing of AuNPs platforms.[19] Likewise, owing to the incorporating of PEI polymer with various inorganic NPs, the therapeutic potential of nanosystems for biological activities can be meaningfully enhanced through their physical characteristics.[20–22] In sum, the application of gold nanoparticle (AuNPs) and PEIs can enhance the signal rate, which lead to increases of intensity and prompting us to investigate the significant role of the dendrimer building of PEIs, AuNPs and GO as the suggested matrix for electro-oxidation of CFX. Given the properties of the nanostructures applied in the proposed polymer substrate, it is estimated that the interaction area of the target with the modified electrode will be significantly amplified.

So, a novel electrochemical aptasensor toward monitoring of CFX residues in milk samples was developed. As seen in Scheme 1, the GO-PEI-AuNPs nanocomposite with good hydrophilic and charged property was fabricated on the Au electrode surface *via* drop casting methods. The modified surface was activated with 1-ethyl-3-(3-dimethylaminopropyl) carbodiimide and *N*-hydroxysuccinimide (EDC/NHS) to fix the aminated CFX aptamer. The AuNPs can be continually encapsulated in GO-PEI matrix by amino-Au affinity, which shows smaller particle size and excellent dispersive stability compared with the AuNPs without a template. So, a well-organized substrate with large surface area and abundant anchor sites for the aptamer attachment was developed. We examined the electrochemical characteristics of GO-PEI-AuNPs platform on Au electrode step-by-step using cyclic voltammetry (CV). The interface construction and polymerization were also tested *via* high-resolution field emission scanning electron microscope (FE-SEM). Then, the GO-PEI-AuNPs/AuE modified electrode conjugated to a specific amine-labeled aptamer *via* EDC/NHS chemistry and amino-Au affinity coupling. After aminated aptamer attachment, the GO-PEI-AuNPs/AuE capability for CFX screening was assessed by square wave voltammetry (SWV) and differential pulse voltammetry (DPV) techniques.

The achieved outcomes proved that the proposed novel aptasensing assay has a suitable sensitivity in sensing of CFX with an acceptable limit of quantification (LLOQ) of 10 nM. This work offers a new GO-PEI-AuNPs-based electrochemical aptasensing strategy to cope with food quality control, and will be broadly considered to determine other targets *via* attaching of numerous aptamer strands. Moreover, the aptasensor exhibited good performance in direct analysis of real milk samples, signifying its promising application in monitoring of complex food matrices.

2. Experimental

2.1. Reagents and materials

The CFX aminated aptamers used in this experiment have been obtained from Bioneer (South Korea) with the following sequences:[23]

(5′-NH_2 modified) 5′-ATACCAGCTTATTCAATTGCAGGG TATCTGAGGCTTGA

TCTACTAAATGTCGTGGGGCATTGCTATTGGCGTTGATACG TACAATCGTAA

TCAGTTAG-3′.

The polyethyleneimine (PEI, branched, M_w 10 000) and graphene oxide (GO) powder were ordered from Sigma-Aldrich (Shanghai, China). Tris–HCl (hydroxymethyl), MCH (mercaptoethanol), disodium hydrogen orthophosphate, potassium ferrocyanide $K_4Fe(CN)_6$, potassium ferricyanide $K_3Fe(CN)_6$, hydrogen tetrachloroaurate(III) hydrate ($HAuCl_4 \cdot 3H_2O$), potassium chloride (KCl), serine, valine, cysteine, methionine, and glutamine were acquired from Merck (Darmstadt, Germany). Supporting electrolyte was freshly prepared at pH = 7.4 in concentration of 0.01 M $K_4Fe(CN)_6/K_3Fe(CN)_6$ (1 : 1) with 0.1 M KCl solution. Other reagents and chemicals were of analytical grade and utilized without further purification. Local and pasteurized milk samples from different supermarkets were randomly collected in Tabriz, Iran.

2.2. Instruments

The AUTOLAB device with PGSTAT302N (Eco Chemie, Utrecht, The Netherlands), driven with NOVA1.11 software was used to perform all the electrochemical experiments. A standard three-electrode cell arrangement was engaged in all electrochemical tests, which consisting of a modified gold electrode (AuE) ($d = 2$ mm) (from Azar electrode Co., Iran) acting as the working electrode, a Ag/AgCl as a reference electrode and Pt wire as a counter-electrode (Methrom, The Netherlands) respectively. The cell is a one compartment cell with 10 mL internal volume. The chemical composition and morphology of the modified surfaces was directly analysis using field emission scanning electron microscope (FE-SEM) which was carried out on a TESCAN system of FEG-SEM MIRA3 TESCAN (Brno, Czech Republic). The energy-dispersive X-ray spectroscope (EDS) of MIRA3 TESCAN (Brno, Czech Republic) model was also used for the electrode surface analysis. Also, the FE-SEM, Transmission electron microscopy (TEM), Philips-CM30, Adelaide, Australia, with an operating voltage of 200 kV, and UV-Vis absorption spectra using a U-3010 spectrophotometer (Hitachi, Japan) have been applied to characterized the constructed GO-PEI-AuNPs nanocomposite.

3. Preparation of GO-PEI-AuNPs nanocomposite

For the synthesis of nanocomposite, 2 mg of the prepared GO distributed in 10 mL of deionized water and sonicated for

20 min to form a uniformly homogeneous GO solution. Then, 0.5 mL of 20 mM $HAuCl_4$ and 3 mL of 5% PEI aqueous solution have been successively added dropwise to the above solution, and the aforesaid mixture solution was placed in water bath at 70 °C. After completing the reaction for 4 h, the GO/PEI/AuNPs nanocomposite was obtained. Finally, the dispersion was stored at room temperature for a long time which no precipitation occurred.

4. Assembly of the modified electrode (aptasensor fabrication)

The diverse steps involved in construction of the GO-PEI-AuNPs/AuE substrate has been presented in Scheme 1. Prior to the electrode modification, the Au electrodes were treated by polishing in cloth pad container 0.3. μm and 0.05 μm of Al_2O_3 powder for 5 min and then rinsed carefully with deionized water. Then, the AuE was further cleaned by ultra-sonication in ultrapure water and 50% ethanol solution to remove organic contaminations. Subsequently, to further eliminating of possible impurities, the cleaning steps were terminated with 12 cycles of cyclic voltammetry (CV) in a 0.1 M H_2SO_4 solution with a potential range of −0.4 to +1.4 V. After cleaning steps, the surface of gold bare electrode was modified with 10 μL of GO-PEI-AuNPs suspension which casted and dried at room temperature to produce a hybrid platform towards aptamer immobilization. The GO functionalization could be done with diverse approaches such as covalent and noncovalent functionalization, and with the nanoparticle's decoration. In this platform, we put forward functionalization of GO by PEI polymer through direct linking of polymeric chains to the graphene sheets. This functionalization can be realized by conjugating GO *via* an amide bond, π–π stacking interactions or electrostatic interaction, obtaining a physiologically stable dual polymer-functionalized nano-GO conjugate with ultra-small size (GO-PEI).[24] Also, the AuNPs can be effectively dispersed on the GO-PEI surface, which in turn this nanocomposite not only improve the signal rate and increase of intensity of signal but also enhance the mechanical properties of film. After that, the modified electrode has been dropped and activated with 10 μL of EDC/NHS (each concentration, 10 mM) solution (pH = 7) for 20 min, followed by rinsing the electrode with excess water. To attach the CFX aptamer, 10 μL of a 5′-aminated aptamer solution in 10.0 mM Tris–HCl (pH 8.0) was immobilized on the GO-PEI-AuNPs/AuE surfaced and incubated at room temperature for 8 h. The unique construction can considerably expand the surface area, and it renders numerous anchor sites for aminated aptamer immobilization. So, the CFX aptamer can be immobilized on the modified electrode through multipoint cross-linking like amino-Au affinity binding and covalent amide bonds by the amino groups on the aptamer and the carboxyl groups on the GO. Afterward, to eliminate any unbounded aptamers, the aptamer modified surface has been accurately washed with phosphate buffer (0.1 M, pH 7.4). Likewise, the Apt/GO-PEI-AuNPs/AuE was immersed in a 1 : 1 ratio of PBS and MCH solution for 30 min to block the any possible remaining nonspecific sites. Finally, the MCH/Apt/EDC-NHS/GO-PEI-AuNPs/AuE surface has been incubated with 10 μL of the CFX solution for 30 minutes. After being rinsed with a phosphate buffer, the label-free CFX aptasensor was denoted as CFX/MCH/Apt/EDC-NHS/GO-PEI-AuNPs/AuE and ready to use.

5. Results and discussion

5.1. Characterization of GO-PEI-AuNPs

The UV-Vis, FE-SEM, and TEM were used to evaluate the optical properties, morphology and the configuration of the synthesis GO-PEI-AuNPs nanocomposites. To prove the successful prepared of GO/PEI/AuNPs nanocomposites by UV-Vis absorption spectra were recorded. As exhibited in Fig. S1A,† GO presents an adsorption bonds at 230 nm corresponding to π–π* electronic transitions of aromatic C–C bonds. After the *in situ* generation of AuNPs on GO-PEI, the strong adsorption bonds appears at 230 nm and adsorption band at 330 nm nearby, which are related to the amine groups in the PEI dendrimer structure and colloidal gold plasmon resonance band, respectively. As given in Fig. S1B, (see ESI†), the long time stability of GO-PEI-AuNPs composites has been evaluated *via* UV-Vis spectroscopy. Although it was expected that the PEI and GO structures can be as appropriate soft nanocontainers for the supramolecular NPs encapsulation through electrostatic or hydrophobic interactions, the signals intensity were declined step by step. Also, the TEM and FE-SEM images were employed to study the surface framework of GO-PEI-AuNPs formation (Fig. 1A and B). The FE-SEM images of GO-PEI-AuNPs show that the AuNPs have been densely decorated with distinctive particle size on a thin layer of crumpled PEI wrapped GO, which demonstrate that the designing of this nanocomposites using PEI and GO sheet as template had well-regulated nanoparticle size. Nevertheless, some nanoparticle aggregation can be seen in the samples that may be directly arises from the amine groups in the PEI structure and the AuNPs surfaces interactions. TEM was also applied, in order to achieve a more perception into the AuNPs coverage onto the PEI wrapped GO and to assess the morphology of GO-PEI-AuNPs nanocomposite. As is well known, the GO have a sheet-like building comprised of large thickness, smooth surface, and wrinkled edges. After combined with PEI polymer, the macroscopic material PEI-GO shows layered construction with reliable shapes and becomes smoother and thicker. It could be obviously seen that the AuNPs are well distributed and its spherical shape with a particle size of about 10–15 nm in PEI-GO structure is obvious. It was interesting to note that the high density AuNPs bind favorably on the PEI surfaces wrapped GO rather than to other regions that are lacking of GO, which in turn it may be owing to the high affinity of AuNPs for the PEI amino groups. PEI polymer could perform either as a stabilizer and a reductant of $AuCl_4^-$ or a primer for the adsorption of $AuCl_4^-$ *via* accelerating the electron transfer from the PEI amine group to Au^{3+}.

5.2. Morphological characterization of modified electrodes

FE-SEM images of bare Au and five modified electrodes in each stage of modification nanoprobe procedure (GO-PEI-AuNPs/

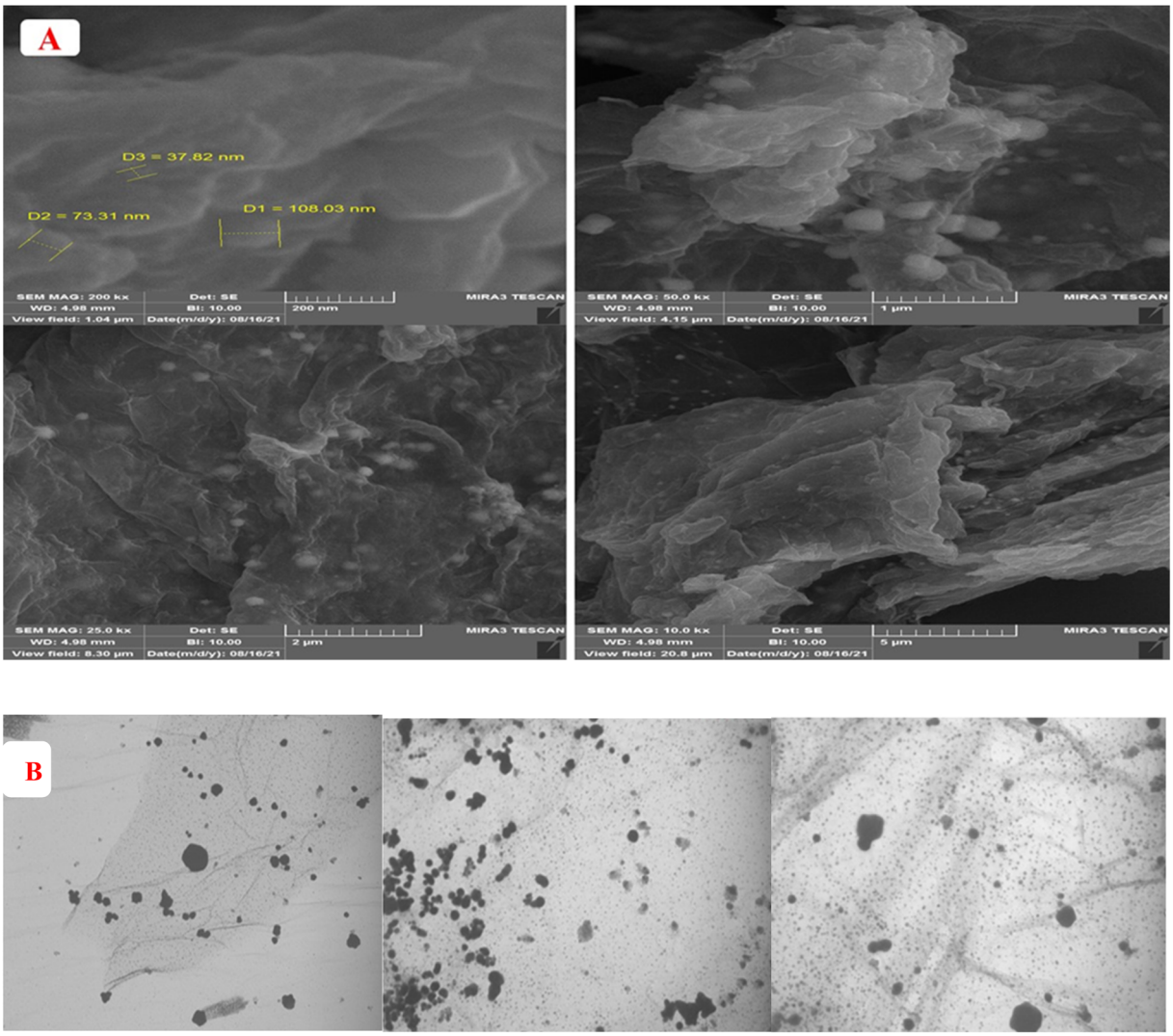

Fig. 1 (A) FESEM image of GO-PEI-AuNPs nanocomposite in different magnifications. (B) TEM image of GO-PEI-AuNPs nanocomposite in different magnifications.

AuE, GO-PEI-AuNPs/AuE, Apt/GO-PEI-AuNPs/AuE, MCH/Apt/GO-PEI-AuNPs/AuE and CFX/MCH/Apt/GO-PEI-AuNPs/AuE) were presented in Fig. S2–S4. (see ESI†). According to the Fig. S2,† compared with bare Au electrode, the GO-PEI-AuNPs thin nanosheet covered on Au electrode revealed wrinkled and rough surface that was very valuable to improve the electroactive area on electrode surface (Fig. S2A and B†). The AuNPs have been densely distributed on the thin layer of crumpled PEI wrapped GO, also suggested platform has good efficiency to immobilize metal nanoparticles. After activation of polymeric substrate with EDC-NHS and immobilization of aminated aptamer, the surface of the GO-PEI-AuNPs composite became rougher and the modified electrode morphology was clearly changed, which indicated that the CFX aptamer can be effectively anchored on the surface of the GO-PEI-AuNPs/AuE. Compared to the GO-PEI-AuNPs/AuE modified electrode, a uniform construction could be designed (Fig. S3A and B†) as a result of the aminated-aptamer and GO-PEI-AuNPs binding through the EDC/NHS chemistry and high affinity of HN–Au. The developed aptamer based bio-assay can detect the CFX with high selectivity and sensitivity (Fig. S4A and B†). To offer supportive insight about FE-SEM images, the EDS, as an effective surface investigation method, was employed to give a confined elementary analysis by means of centralized emitted electrons from a solid sample bombarded as the X-ray spectrum. These spectra are not sophisticated and evaluation of the plots is typically applied for qualitative analysis. As seen in Fig. S5,† the existence of C, O, N, S, and F elements in aptamer assay after binding CFX molecules, confirmed the good performance of designed probes.

5.3. Electrochemical monitoring of CFX aptasensor fabrication

To monitor the construction processes of the aptamer probes after each assembly step, cyclic voltammetry (CV) measurement was implemented in a 0.01 M $[Fe(CN)_6]^{3-/4-}$ solution

comprising 0.1 M KCl as standard redox probe in a potential range of −1.2 to +1.2 V at a scan rate of 100 mV s^{-1}. As seen in Fig. 2, a pair of well-behaved redox peaks have been detected on the bare AuE, which is arises from the superb electron transfer effectiveness between electrode surface and $[Fe(CN)_6]^{4-/3-}$ in solution. The results indicate that the bare AuE has a peak current in 9.64 μA, which can be described to inherent attribute of gold as a conductive metal. In the next step, when the surface of electrode was modified with GO-PEI-AuNPs nanocomposite, the currents and position of cathodic and anodic peak were changed (7.00 μA), which can be confirmed the effective modification of the AuE by this nanocomposite. This changed in kinetics of electron transfer can be related to the presence of GO and AuNPs in the designed substrate. Besides, this probe is recognized to provide a high coupling site, which induce a high dense-loading of aminated aptamers. After activation of functional group of nanocomposites by NHS/EDC and upon the immobilization of the CFX aptamer on the modified electrode *via* EDC/NHS chemistry and HN-Au binding, an obvious decline in the currents of cathodic and anodic peak were observed (4.43 μA) owing to the creation of an insulating biological layer, which impended the electrons transfer.[10–15] Finally, when CFX was drop casted on the surface of Apt-modified electrode, the peak current also lightly declined (4.03 μA), indicating the assembly of Apt/CFX complex on interface of the electrode surface. Upon the addition of CFX molecule a conformational change was induced, Apt was folded and Apt/CFX complex has been arranged, which leads to the physical hindrance following by partially electron transfer inhibition.[13] Likewise, the stability of GO-PEI-AuNPs/AuE interfaces was tested *via* CVs technique using the number of cycles and the results are presented in Fig. S5. (see ESI†). In this regard, CVs have been carried out 100 consequents cycles (5, 10, 20, 30, 50 and 100) in 0.01 M $[Fe(CN)_6]^{3-/4-}$ comprising 0.1 M KCl as mediator solution. According to the experimental data, the GO-PEI-AuNPs/AuE composite is entirely stable. CVs explores that with increasing of CV cycles, there is no considerable decrease in the current of peak's.

5.4. Kinetic analysis

Scan rate can be applied as a significant parameter in the assessment of redox reactions for selected analytes, moreover valuable data containing electrochemical kinetics of electron transfer could be acquired from the association between the potential to sweep rate and peak's current.[25,26] Hence, the typical CVs at different scan rate (10–1000 mV s^{-1}) with determined potential range (−1.2–+1.2 V) have been employed to evaluate the interface surface kinetic (GO-PEI-AuNPs/AuE) in 0.01 M of $K_3Fe(CN)_6$ solution and dependency plot was presented in Fig. 3. Additionally, the graph of oxidation linear peak currents to sweep rate displayed in Fig. 3A and B implying the electrochemical activity of designed surface.

$$I_p = (n^2F^2/4RT)\nu A\Gamma^*$$

where I_p is the peak current, A the electrode surface area ($A = \pi r^2 = 0.0314$ cm^2), ν is the potential sweep rate and the surface

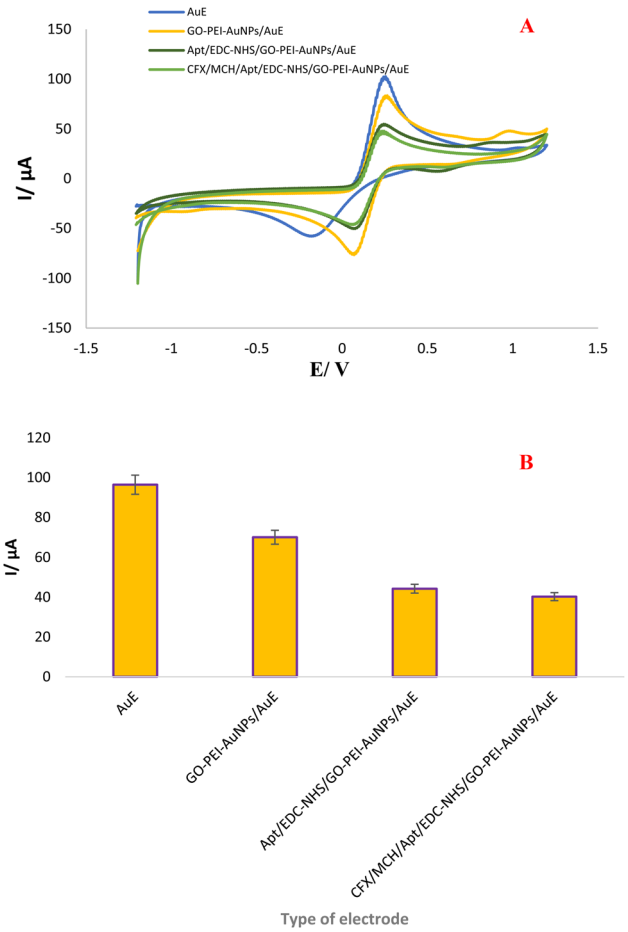

Fig. 2 (A) CVs of AuE, GO-PEI-AuNPs/AuE, Apt/GO-PEI-AuNPs/AuE, and CFX/MCH/Apt/GO-PEI-AuNPs/AuE in a solution comprising 0.01 M $[Fe(CN)_6]^{3-/4-}$ with 0.1 M KCl as redox probe in a potential range of −1.2 to +1.2 V at a scan rate of 50 mV s^{-1}. (B) Histogram of current of plot *versus* various modification steps.

coverage of the redox species determined with Γ^* that can be calculated as 1.67×10^{-9} mol cm^{-2}. Based on the linear relationship between the peak currents *versus* square root of scan rate in the various range from 10 to 1000 mV s^{-1}, it can be explored that the electrooxidation GO-PEI-AuNPs nanocomposite was diffusion-controlled. Similarly, ln I_p *versus* ln ν plot analysis is used as another technique to examine the reversibility of reactions and determine whether the change transfer was performed by irreversible process. Also, the association of ln I_{pa} *vs.* ln ν was linear and defined by the following equation:

$$\ln I_{pa} = 0.4623 \ln \nu\ (\mathrm{V\ s^{-1}})\ 2.4027\ \mu\mathrm{A}\ (R^2 = 0.993)$$

The slop is 0.4623, which confirms the control of the procedure with diffusion. In view of the E_{pa} *versus* ln ν for the GO-PEI-AuNPs/AuE substrate, it could be said that the type of coupled reaction method was irreversible as the positions of peak potential are changed as a function of scan rate. In sum, it can be concluded that the electrochemical redox process is irreversible and diffusion-controlled.

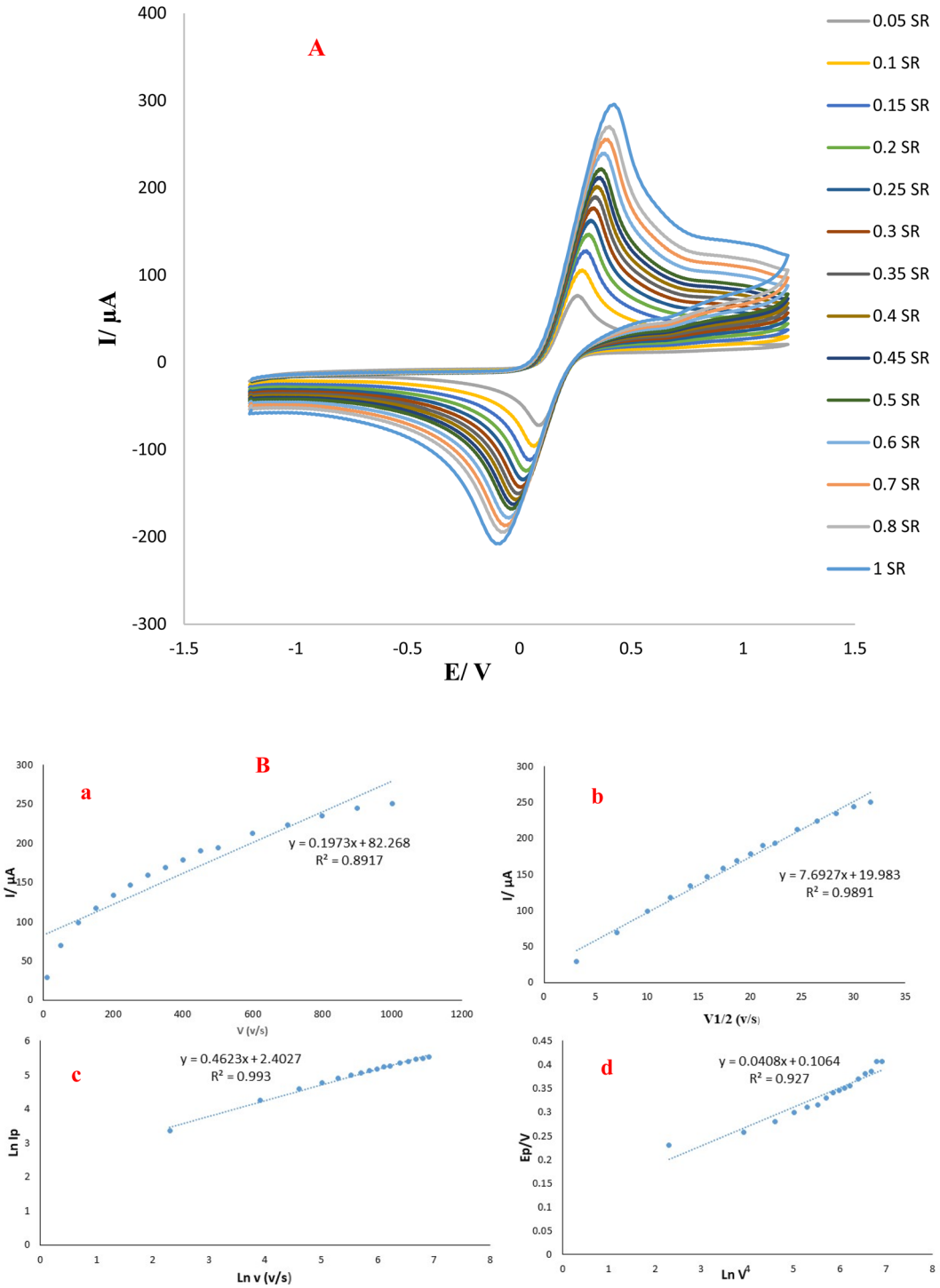

Fig. 3 (A) CVs of GO-PEI-AuNPs/AuE in the presence of 0.01 M $[Fe(CN)_6]^{3-/4-}$ with 0.1 M KCl, in various potential scan rates (20–1000 mV s^{-1}). (B) (a) Relationship between oxidation peak currents *versus* sweep rates CVs, (b) calibration curve of oxidation peak currents based on square root of different sweep rate, (c) relationship between the Neperian logarithm of I_{pa} (ln I_{pa}) and Neperian logarithm of scan rate (ln *v*), (d) dependency of peak potential *versus* Neperian logarithm of sweep rates.

5.5 Optimization of experimental condition

The quantitative and qualitative sensitivity of the suggested electrochemical aptasensor can be affected through the detection conditions. In this prospect, to acquire the best sensing responses for CFX identification, some experimental factors like the aptamer immobilization time, aptamer concentration, and reaction time of CFX have been optimized in the aptasensor designing process (CFX/MCH/Apt/GO-PEI-AuNPs/AuE) using CV technique. The assembly amount of aptamer and aptamer assembly time have an imperative role in the maximize the

electrochemical signals of the suggested substrate. In light of this, different amount of aptamer solution were tested to fulfill a high coverage of the GO-PEI-AuNPs/AuE surface with aminated aptamers for efficiently sensing of CFX. The effective amount of aptamer was explored *via* casting three concentrations of the aptamer (5.0, 10, and 15 μM) on the surface of electrode. As depict in Fig. S6(A, B†). The 10 μL of aptamer as optimal value was applied in the subsequent studies. The peak current step by step enhanced when the aptamer assembly time from 4 h to 8 h, demonstrating an orientation to saturate the interaction with CFX (Fig. S6C, D†). Afterward, increasing the time no longer increases the response signal. It can be ascribed to the reactive sites saturation on the GO-PEI-AuNPs/AuE surface after determined period. Hence, in order to obtain the good performance of the designed aptasensor, the 10 μL and 8 h as have been chosen as optimum amount and time in this research, respectively. What's more, reaction time of CFX will also affect the electrochemical signal and detection sensitivity. Reaction time in aptamer based sensor is mentioned to as the minimum time needed for the aptamer-target conjugate interaction, and it can be influenced by the DNA properties (*e.g.*, DNA sequence length).[27] As expected, longer reaction times lead to better determination efficiency. This optimization intended to describe the reaction time that is both rapid and satisfactorily efficient. Thus, the effect of target reaction time on the modified electrode has also been examined from 10 to 60 minutes. In this study, CFX (10 μL, 100 nM) was drop cast on MCH/Apt/GO-PEI-AuNPs/AuE surface. Fig. S6(E, F†) displays that the total current response was meaningfully intensify through an increase in the incubation time up to 30 minutes and then decline, signifying that the CFX-aptamer conjugate formation can be completed after 30 min. Thus, 30 min was intended as optimal time for the further experiments.

5.6. Analytical approach

To investigate the quantitative elements involved in CFX assessment at the MCH/Apt/GO-PEI-AuNPs/AuE surface, the limit of detection, sensitivity, and linear range have been explored using DPV technique. The DPV and SWV techniques as a result of high sensitivity were used for the efficiently quantitative analysis of CFX. Hence, DPV and SWV were employed to detection of CFX under determined potential range of −1.2 to +1.2 V with 0.1 V of interval time. The aptamer bound modified electrode (MCH/Apt/GO-PEI-AuNPs/AuE) was incubated with various concentration of CFX (100, 10, 1, 0.1, 0.01 μM) for 30 min and then determined in 0.01 M solution of $K_3Fe(CN)_6$ with 0.1 M KCl. Fig. S7(A–D†) presents the DPVs and SWVs responses of aptasensor toward different CFX concentrations with the corresponding calibration plot. As revealed in the DPV and SWV voltammograms, well defined peaks in the CFX range of 0.001 to 100 μM were acquired. It could be explained that upon CFX addition, the peak current of oxidations of $Fe^{(III)}/Fe^{(IV)}$ were rises. The linear responses have also been obtained once the concentrations of CFX are within the range of 10 nM to 100 μM. Also, the low limit of quantification (LLOQ) is considered to be ∼10 nM. Table 1 (ref. 28–32) summarized some of the analytical parameters for the measurement of CFX using the suggested aptasensor and other aptasensors. Compared with the previous reports, the developed aptamer based sensor offers benefits in simple operation, rapid analysis, easy fabrication, and high sensitivity. Real-time analysis is also possible for our designed probe.

5.7. Analysis of local and pasteurized milk samples (real sample analysis)

The practical usefulness of the CFX aptasensor was tested by quantifying the CFX residues in two milk samples, including

Table 1 Summaries of our suggested aptasensor performance with some other described approaches

Sensor fundamentals	Approach/ detection	Detection method	Analytical factors	Sample	Ref.
Based on the core–shell fluorescent molecularly imprinted nanoparticles@SiO_2-FITC	Fluorescence	—	DL = 4.04 nM LR = 0–250 nM	Aquaculture water	28
Aptasensor was based on CNT-molybdenum diselenide ($MoSe_2$) platform	Fluorescence-labeled	—	DL = 0.63 ng mL^{-1} LR = 0.63–80 ng mL^{-1}	Milk	29
Molecular imprinting-solid phase extraction	Liquid chromatography	—	DL = 0.019 M	Milk	30
The electrochemical aptamer assay was developed using carbon nanotube (CNT)-V_2O_5-chitosan substrate	Label-free	EIS ($Fe(CN)_6^{3-/4-}$)	DL = 0.5 ng mL^{-1} LR = 0.5–8.0 ng mL^{-1}	Milk	31
An aptasensor was fabricated on to the AuE electrode by means of single-stranded DNA-binding protein (SSB)	Labelled electrochemical	CV ($Fe(CN)_6^{3-/4-}$)	DL = 336, 351 and 261 pM LR = 800 pM to 400 nM	In serum, milk and water	32
An aptasensor was designed based on graphene oxide-nanogold-functionalized branched polyethyleneimine composite	Label-free electrochemical	CV, DPV, SWV ($Fe(CN)_6^{3-/4-}$)	DL = 1 nM LR = 10 nM −100 μM	Local and pasteurized milk	This study

pasteurized and local milk which purchased from a local supermarket. Based on direct analysis by electrochemical method, it is worth remarking that the sample pretreatment and extraction was not needed, which is an outstanding operational feature of the aptasensor considering these detections are mainly challenging owing to the matrix complexity of milk samples. Prior to the start of investigate, contaminated milk solutions by different CFX concentration (100, 50, 10, 1 M, 0.1, 0.01 and 0.001 μM) have been prepared using spiking a standard solution of CFX to the milk samples. Then, 10 μL of prepared samples with defined CFX concentration were introduced on the surface of a MCH/Apt/GO-PEI-AuNPs/AuE substate. Afterward, the DPVs and SWVs in 0.01 M $K_3Fe(CN)_6$ with 0.1 M KCl solution as the supporting electrolyte were implemented under optimal conditions for analyzing of CFX in local and pasteurized milk samples (Fig. 4 and 5). Using proposed platform and SWV and DPV technique, the peak current of oxidations of Fe(III)/Fe(IV) was decreased with CFX concentration increment. The obtained results revealed that this platform is able to measure CFX residue in the concentration range of 0.001 to 100 μM in milk samples with the related calibration curves plotted the linear regression equation to DPVs and SWVs are as follows:

Linear regressions equation obtained from DPVs investigation in local and pasteurized milk sample:

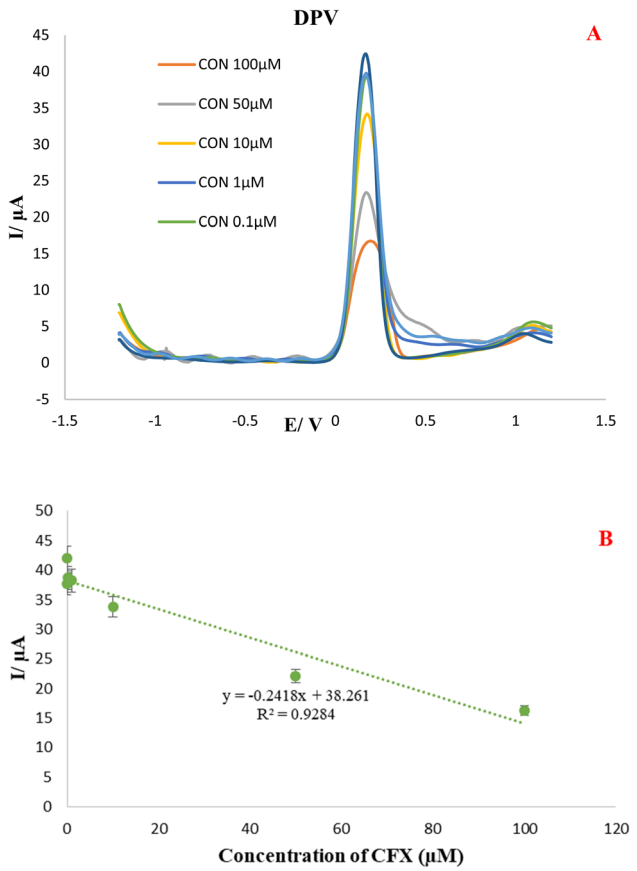

Fig. 4 (A). DPVs of Apt/GO-PEI-AuNPs/AuE proposed aptasensor in the presence of different CFX concentration (100, 50, 1, 0.1, 0.01 and 0.001 μM) in local milk samples. (B) Calibration curve.

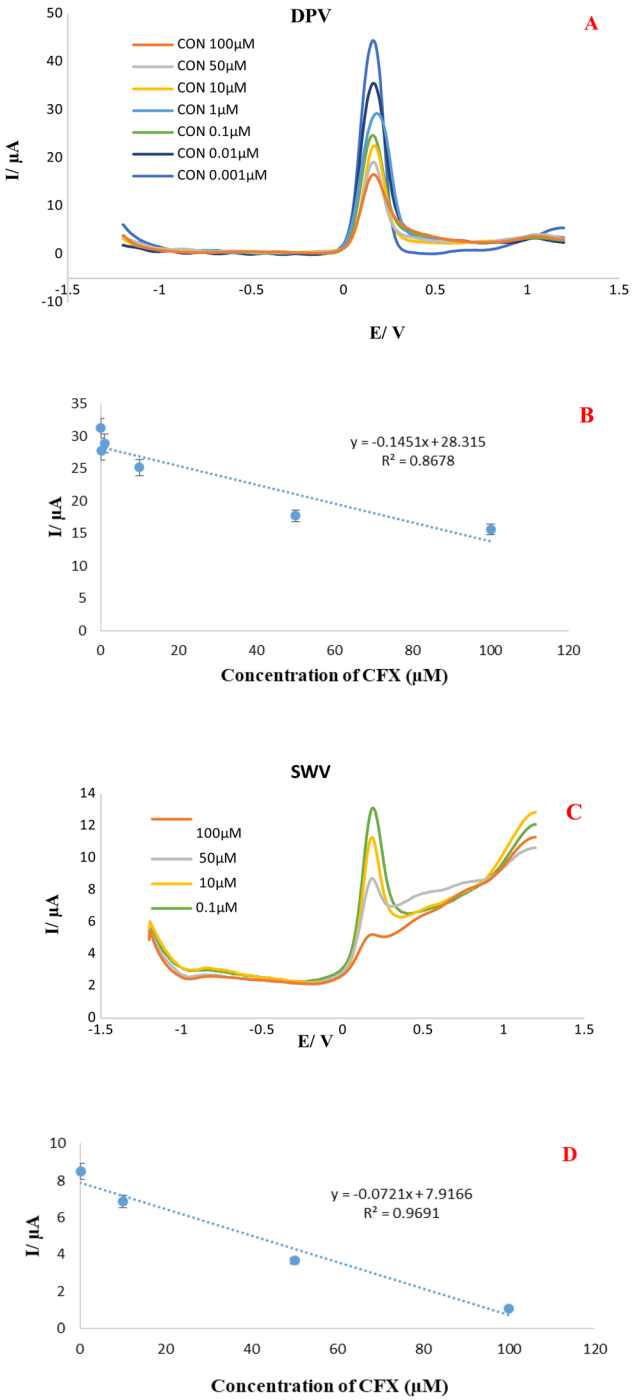

Fig. 5 (A & B). DPVs and SWVs of Apt/GO-PEI-AuNPs/AuE proposed aptasensor in the presence of different CFX concentration in pasteurized milk samples (B) calibration curve.

$$I_p\ (\mu A) = -0.2418C_{(CFX)} + 38.261,\ R^2\ 0.9284.\ \text{(Local milk)}$$

$$I_p\ (\mu A) = -0.1451C_{(CFX)} + 28.315,\ R^2\ 0.8678.\ \text{(Pasteurized milk)}$$

Linear regressions equation obtained from SWVs investigation in local and pasteurized milk sample:

$$I_p\ (\mu A) = -0.3181C_{(CFX)} + 41.139,\ R^2\ 0.874.\ \text{(Local milk)}$$

I_p (μA) = −0.0721$C_{(CFX)}$ + 7.9166, R^2 0.9691. (Pasteurized milk)

Besides, the well-defined DPV and SWVs responses are indicate for each milk samples with an acceptable LLOQ (1 nM). The accurate monitoring of CFX in local and pasteurized milk sample with good specificity and satisfactory repeatability implied promising practical feasibility of the MCH/Apt/GO-PEI-AuNPs/AuE modified electrode in foodstuff. Finally, our established apta-platform performance was compared with the analytical performance some previously reports electrochemical and non-electrochemical method about CFX detection in different matrices and results were mentioned in Table 1. According to the table our apta-platform is competitive in the terms of modification and recognition time, LOD, and linear rang.

5.8. Specificity, stability, and reproducibility of the designed aptasensor

Specificity performance is an imperative index for measuring the efficiency of the suggested CFX aptasensor. Pasteurized and local milk samples typically contain vitamins, amino acids, lactose, and ions. In order to evaluate the anti-interference capability of the aptasensor, the influence of these coexisting elements like serine, valine, cysteine, methionine, and glutamine on the test of CFX were studied by DPVs techniques. Their concentrations are 10-folds compared with CFX concentration. As results are shown in DPVs voltammogram (Fig. S8 (see ESI†)), the peak's currents acquired from CFX have been compared with interferer species. The results prove that serine, valine, methionine, and glutamine has no interfere in CFX detection, while, cysteine decreasing intensity of CFX peak's currents, indicating that the fabricated aptasensor exhibits a satisfactory selective recognition function for CFX residue. The high sensitivity and good specificity of this sensing substrate can be stem from the high selectivity of CFX aptamer and its high binding affinity toward CFX molecule (K_D = 0.1–56.9 nM), respectively.[23] What's more, we further evaluated the stability of the designed aptamer assay by inter-and intra-day precision examines. Under optimized experimental conditions, the inter-and intra-day precision has been tested at the 100 nM concentration of CFX. Inter-day stability of aptamer probe was monitored *via* CVs voltammogram 9 times within a day in the almost interval times and similar conditions. The peak currents for both reduction and oxidation experienced an insignificant decreases. Besides, inter-day precision of aptasensor was implemented over seven days. The AuE modified (MCH/Apt/EDC-NHS/GO-PEI-AuNPs/AuE) was kept at room temperature and CV test has been performed every 24 hours. According to Fig. S9(A–D) (see ESI†), the highest peak current was obtained on the first day. Afterward, the current of voltammogram was altered constantly through the next days. In sum, the suggested platform has stable sufficient.

6. Conclusion

In this study, we have successfully synthesized a label-free electrochemical aptasensor using MCH/Apt/GO-PEI-AuNPs/AuE for signal enhancement to achieve facile, rapid and directly detected of CFX in local and pasteurized milk samples. Herein, the GO-PEI-AuNPs nanocomposite was prepared and used as an efficient solid support on the AuE surface, which not only enhance electrochemical signal and accelerate the electron transfer rate, but also offer a larger specific surface area for the immobilization of aptamer. Indeed, the GO nanosheets can offer plentiful sites toward PEI molecules, and acte as a soft matrix to improve the stability of attached aminated aptamer. The engineered nanoprobe has satisfactory selective recognition function toward CFX even in the presence of high concentration of coexisting elements *via* DPV technique. Acceptable linear range of 0.001 to 100 μM with relatively low detection limit of 0.001 μM were obtained in the milk samples analysis which demonstrated the hopeful practicality of the developed aptasensor for other antibiotics residues in dairy product. Regardless of the promising performance, key aspects to focus more works comprise the amalgamation of this assay with multiplexing platforms permitting the simultaneous target analysis in various fields, especially for food safety.

Ethical issues

This study was ethically approved (IR.TBZMED.VCR.-REC.1398.470) by Tabriz University of Medical Sciences.

Conflicts of interest

The authors declare no conflict of interests.

Acknowledgements

The authors are grateful for the financial support provided by the Tabriz University of Medical Sciences, Tabriz, Iran. Also, we thanks Pharmaceutical Analysis Research Center, Tabriz University of Medical Sciences, as site of experimental research work.

References

1 R. Mirzaei, M. Yunesian, S. Nasseri, M. Gholami, E. Jalilzadeh, S. Shoeibi and A. Mesdaghinia, *Sci. Total Environ.*, 2018, **619**, 446–459.
2 C. Vakh, A. Pochivalov, S. Koronkiewicz, S. Kalinowski, V. Postnov and A. Bulatov, *Food Chem.*, 2019, **270**, 10–16.
3 R. M. Kalunke, G. Grasso, R. D'Ovidio, R. Dragone and C. Frazzoli, *Microchem. J.*, 2018, **136**, 128–132.
4 W. Lu, Y. Jiao, Y. Gao, J. Qiao, M. Mozneb, S. Shuang, C. Dong and C.-z. Li, *ACS Appl. Mater. Interfaces*, 2018, **10**, 42915–42924.
5 M. Mahmoudpour, A. Saadati, M. Hasanzadeh and H. Kholafazad-kordasht, *J. Mol. Recognit.*, 2021, e2923.
6 M. Mahmoudpour, H. Kholafazad-kordasht, J. E. N. Dolatabadi, M. Hasanzadeh, A. H. Rad and M. Torbati, *Anal. Chim. Acta*, 2021, 338736.
7 J. Pang, Y. Liao, X. Huang, Z. Ye and D. Yuan, *Talanta*, 2019, **199**, 499–506.

8 K. Rudnicki, K. Sipa, M. Brycht, P. Borgul, S. Skrzypek and L. Poltorak, *TrAC, Trends Anal. Chem.*, 2020, **128**, 115907.
9 L. V. de Faria, T. P. Lisboa, N. da Silva Campos, G. F. Alves, M. A. C. Matos, R. C. Matos and R. A. A. Munoz, *Anal. Chim. Acta*, 2021, 338569.
10 Z. Han, Z. Tang, K. Jiang, Q. Huang, J. Meng, D. Nie and Z. Zhao, *Biosens. Bioelectron.*, 2020, **150**, 111894.
11 M. Mahmoudpour, J. E. N. Dolatabadi, M. Torbati, A. P. Tazehkand, A. Homayouni-Rad and M. de la Guardia, *Biosens. Bioelectron.*, 2019, **143**, 111603.
12 M. Mahmoudpour, S. Ding, Z. Lyu, G. Ebrahimi, D. Du, J. E. N. Dolatabadi, M. Torbati and Y. Lin, *Nano Today*, 2021, **39**, 101177.
13 A. Joshi and K.-H. Kim, *Biosens. Bioelectron.*, 2020, **153**, 112046.
14 M. Mahmoudpour, Z. Karimzadeh, G. Ebrahimi, M. Hasanzadeh and J. Ezzati Nazhad Dolatabadi, *Crit. Rev. Anal. Chem.*, 2021, 1–28.
15 C. Zhou, H. Zou, C. Sun and Y. Li, *Food Chem.*, 2021, 130109.
16 W. Chen, Z. Wang, S. Gu, J. Wang, Y. Wang and Z. Wei, *Sens. Actuators, B*, 2020, **306**, 127579.
17 J. J. Virgen-Ortíz, J. C. Dos Santos, Á. Berenguer-Murcia, O. Barbosa, R. C. Rodrigues and R. Fernandez-Lafuente, *J. Mater. Chem. B*, 2017, **5**, 7461–7490.
18 T. Ishii, H. Otsuka, K. Kataoka and Y. Nagasaki, *Langmuir*, 2004, **20**, 561–564.
19 V. K. Ponnusamy, V. Mani, S.-M. Chen, W.-T. Huang and J.-F. Jen, *Talanta*, 2014, **120**, 148–157.
20 V. Mulens-Arias, A. Nicolás-Boluda, A. Gehanno, A. Balfourier, F. Carn and F. Gazeau, *Nanoscale*, 2019, **11**, 3344–3359.
21 M. Jafari, M. Hasanzadeh, R. Karimian and N. Shadjou, *Microchem. J.*, 2019, **147**, 741–748.
22 B. Adel, M. Jafari and M. Hasanzadeh, *J. Mol. Recognit.*, 2021, e2900.
23 C. Reinemann, U. F. Von Fritsch, S. Rudolph and B. Strehlitz, *Biosens. Bioelectron.*, 2016, **77**, 1039–1047.
24 V. P. Jain, S. Chaudhary, D. Sharma, N. Dabas, R. S. K. Lalji, B. K. Singh and G. Jaiswar, *Eur. Polym. J.*, 2021, **142**, 110124.
25 S. Hassanpour, A. Saadati, M. Hasanzadeh, N. Shadjou, A. Mirzaie and A. Jouyban, *Microchem. J.*, 2019, **145**, 266–272.
26 M. Hasanzadeh, S. Hassanpour, A. Saadati, N. Shadjou and A. Mokhtarzadeh, *Nano LIFE*, 2017, **7**, 1750006.
27 S. Forouzanfar, F. Alam, N. Pala and C. Wang, *J. Electrochem. Soc.*, 2020, **167**, 067511.
28 C. Wu, R. Cheng, J. Wang, Y. Wang, X. Jing, R. Chen, L. Sun and Y. Yan, *J. Sep. Sci.*, 2018, **41**, 3782–3790.
29 X. Hu, P. Wei, G. Catanante, Z. Li, J. L. Marty and Z. Zhu, *Microchim. Acta*, 2019, **186**, 1–8.
30 H. Yan, M. Tian and K. H. Row, *J. Sep. Sci.*, 2008, **31**, 3015–3020.
31 X. Hu, K. Y. Goud, V. S. Kumar, G. Catanante, Z. Li, Z. Zhu and J. L. Marty, *Sens. Actuators, B*, 2018, **268**, 278–286.
32 K. Abnous, N. M. Danesh, M. Alibolandi, M. Ramezani, S. M. Taghdisi and A. S. Emrani, *Sens. Actuators, B*, 2017, **240**, 100–106.